Shape Memory Silicone Using Phase-Changing Inclusions

Trevor L. Buckner[1], Michelle C. Yuen[1], Rebecca Kramer-Bottiglio[1]

Abstract— **Functional, responsive materials are attractive for use as key components in soft robots as they can replace otherwise rigid or bulky parts. In this work, we present a functional silicone with shape memory properties that, due to the retention of elasticity and flexibility, can be seamlessly integrated into the body of a soft robot. By dispersing particles of low-melting-point metal alloy (Field's metal) into a silicone matrix, the resulting composite can be "frozen" into various shapes by sequentially heating to melt the Field's metal particles, stretching the composite, and cooling to solidify the Field's metal particles in the deformed configuration. The ramifications of this operational capability include both stiffness control and 3D shape reconfiguration. In this paper, we characterize the thermomechanical behavior and shape memory performance of the Field's metal/silicone composite. We then highlight applications of the material to impedance and trajectory control, and topography recording.**

I. INTRODUCTION

Much of soft robots' flexible nature is possible through the adoption of actuators, sensors, and stiffness control mechanisms that leverage the functionality of responsive materials. Such materials can often be made into flexible, monolithic analogs of rigid, multi-part components, and when combined with other materials in composite, may become responsive to more than one stimulus. In many cases, these materials can be used simultaneously as the body of the robot itself. This capacity to perform multiple functions with the same material can allow for drastically lowered part counts, simplified manufacture, and mass reduction. In the field of soft robotics, responsive materials have been widely used for actuation (NiTi shape memory alloys, hydrogels, liquid crystal elastomers [1], [2]), sensing (piezoresistive [3], temperature [4]), and stiffness control (thermoplastics [5], low-melting-point alloys [6]). However, challenges remain in integrating many of these responsive materials seamlessly with soft robotic structures due to material property mismatch. Soft robots are most commonly constructed from silicone due to its high flexibility, yield strain and elastic cyclability. Responsive silicones in particular, then, become an ideal material for use in soft robotic components.

Multifunctional silicone elastomers generally take the form of a composite, with the additional functionality arising from the filler material. Most commonly, silicone elastomers have been loaded with electrically conductive fillers including carbon-based nanomaterials [7], expanded intercalated graphite [8], metal nanowires [9], and liquid metal [10] to create stretchable conductors or sensors. Similarly, enhanced

[1] School of Engineering & Applied Science, Yale University, New Haven, CT, USA. email: {trevor.buckner, michelle.yuen, rebecca.kramer}@yale.edu
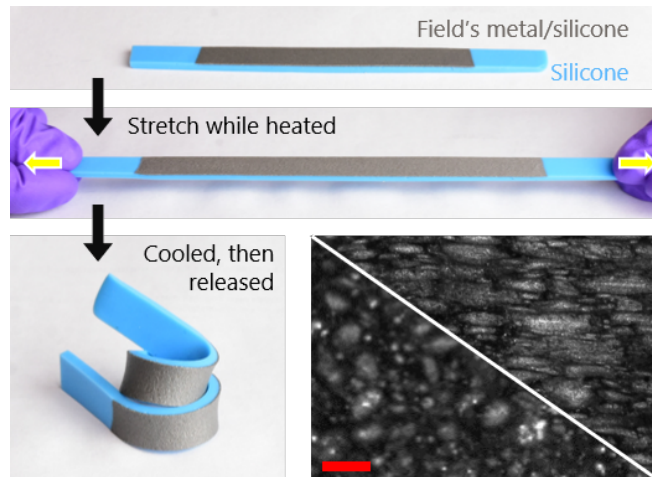
Fig. 1. Field's metal particles are embedded in silicone for shape memory applications. Here, Field's metal/silicone composite (gray) is bonded to native silicone (blue). After melting the Field's metal, the composite is stretched. Upon solidification of the Field's metal, the composite retains the applied elongation, resulting in a curled bilayer structure as the native silicone contracts to its original length. Width of the specimen is 1cm. Microscope images of the composite show the morphologies of the Field's metal particles in the unstrained (bottom left) and strained (top right). Scale bar is $200\mu m$.

and anisotropic thermal conductivity can be achieved by shear mixing liquid metal into elastomers [11]. To achieve actuation using a silicone-based composite, magnetic fillers have been mixed into elastomers and programmed to respond to external magnetic fields [12], [13], and ethanol has been mixed into silicone to serve as a thermally-responsive volumetrically-expanding actuator [14]. For stiffness change, functional inclusions include iron microparticles and magneto-rheological fluid which have been used to create magnetoactive elastomers that stiffen in the presence of a magnetic field [15], [16], thermoplastics that undergo glass transition [17] [18], and low-melting-point alloys that undergo solid-liquid phase change [19]–[21].

The ability to change the stiffness of silicone has close ties to shape memory capabilities. Shape memory broadly refers to the ability to trigger a return to a programmed state after being manipulated [22]. Shape memory in elastomers has been demonstrated previously using liquid crystal elastomers [23] and semi-crystalline elastomers [24], [25]. Other approaches involve embedding percolating networks of cellulose nanofibers in an elastomer matrix [26] and preparing a polymeric gel network filled with a supercooled salt solution [27]. Shape memory behavior has been used to reversibly program 3D shapes into 2D planar materials [28]
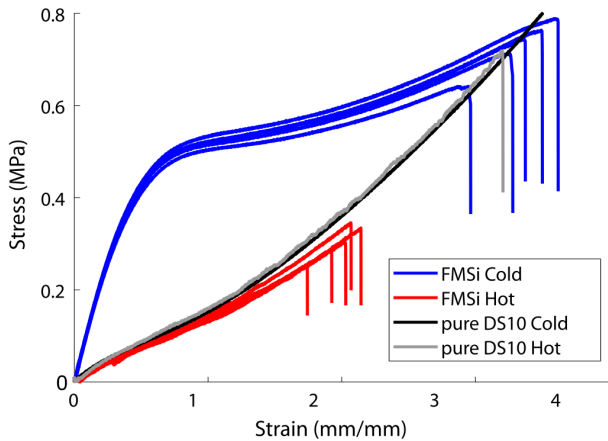
Fig. 2. Thermomechanical behavior of FMSi under pull-to-failure tests. Stress vs. strain plots of FMSi in cold (FM solid) and hot (FM liquid) states show drastic differences in stiffness and failure strain.

notably via thermally-responsive [29] and humidity-sensitive materials [30], or stress-driven assembly [31].

We build upon our previous work with Field's metal/silicone (FMSi) composites, where we showed that the modulus and stretchability can be switched through the solid-liquid phase change of the Field's metal [32]. The solid-liquid phase change, in combination with the stretchability of the silicone matrix enabled "stretch-and-hold" operations where the composite could be heated, stretched, and then cooled in place to maintain a strained configuration. The work presented here more directly explores this stiffness-changing material as a source of shape memory behavior (Fig. 1). By adjusting the degree and direction of strain during the shape-fixing process, we can thermomechanically program different in-plane moduli and achieve anisotropic behavior. We also quantify the ability of FMSi to hold and recover shape, and measure recovery forces which show potential as a stored-energy actuator. Finally, we demonstrate FMSi as an on-demand modulus and shape-changing material with potential for soft robotics applications.

II. MATERIAL CHARACTERIZATION

A. Fabrication

The FMSi composite consisted of 30vol% Field's metal particles and 70vol% silicone (Dragon Skin 10 Medium, Smooth On). The Field's metal particles were fabricated by shear-mixing bulk Field's metal (RotoMetals) in hot water, using the process discussed in [32]. The Field's metal particles and silicone were hand-mixed for approximately 1min to distribute the particles evenly throughout the silicone matrix. The mixture was then cast into a film by blade-coating with a 1mm gap, resulting in a film thickness of approximately $631.4 \pm 10.9\mu$m (mean $\pm$ 1 stdev). With the largest FM particles having a diameter of 355μm after sieving, the thickness of the FMSi film ensured that there would be a sufficient amount of silicone for a continuous matrix, preventing immature rupturing of the film around a single large particle. The film was allowed to cure for

a minimum of 2h after which the films were sliced into rectangular coupons (100mm x 8mm). Microscope images taken of the cross-section showed that the Field's metal particles settled to the bottom into a $474.8 \pm 10.7\mu$m layer, leaving a less dense "supernatant" $156.6 \pm 6.8\mu$m thick layer on top. Fabric reinforcement tabs (20mm x 8mm) were adhered to both ends of each specimen, resulting in a stretchable region of 60mm x 8mm.

Additional compositions of the FMSi can also be used. Changing the volume fraction of FM inclusions affects the stiffness ratio achieved, as discussed in [32]. However, at overly high volume fractions of FM, the films have a tendency to leak when deformed while the FM particles are liquid. Changing the matrix material can affect the stiffnesses in both the hot and cold states, and the curing time, and thus the distribution of FM particles and/or void spaces in the composite. Further work can explore tuning the composition of the FMSi to better suit application requirements.

B. Hot vs. Cold

The thermal effect on tensile behavior of the FMSi was first investigated (Fig. 2). In previous work, we focused on mechanical properties under small bending deformations [32]. Here, we investigate the behavior under much higher strains. Specimens were clamped into a materials testing system (Instron 3345) and pulled to failure at 200% strain/min (120mm/min). FMSi and unmodified silicone samples were tested at room temperature (Cold) and heated to between 80-100°C (Hot). The pure silicone samples showed negligible change in stiffness between the hot and cold states. However, the heated silicone samples failed earlier (300% vs. 800% strain). The stiffness of the hot FMSi sample (172kPa) was similar to that of the pure silicone (186kPa). The cold FMSi sample was initially much stiffer (976kPa), with a noticeable elbow in the stress-strain curve occurring at approximately 70% strain, followed by a lower stiffness region (59kPa). We hypothesize that this lower stiffness region corresponds to the debonding regime, where the silicone matrix has separated from the Field's metal particles. When not pulling to failure, preliminary results (not shown here) suggest that the cyclic strain behavior of the FMSi exhibits little change in stress-strain response between cycles, similar to that of neat silicone. However, we did observe that at higher strains beyond the debonding limit, there was a high degree of hysteresis on the initial cycle of strain, exceeding the characteristic Mullens effect that was observed in neat silicone, followed by negligible hysteresis in subsequent cycles. We attribute this behavior to the separation of the silicone matrix from the FM particles.

C. Pre-strain

After characterizing the effect of the FM's phase on the FMSi's mechanical properties, we then held the FMSi material under strain as the FM cooled from a liquid to a solid state. When the FMSi composite is heated and then strained, any melted, spherical Field's metal microparticles are also stretched along with the surrounding silicone matrix into an
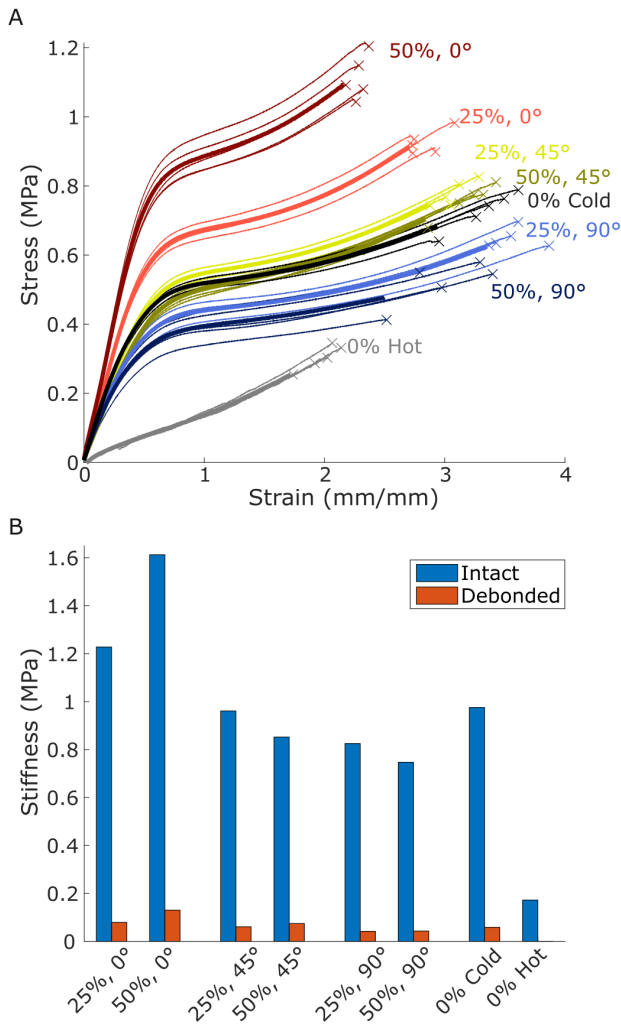
Fig. 3.   Mechanical behavior of pre-strained FMSi under tensile pull-to-failure tests. (A) Stress vs. strain plots of FMSi programmed with pre-strains of 25% and 50%, at three angles (0°, 45°, 90°) with respect to the loading direction. Specimens were pulled to failure at 200% strain/min. (B) Stiffnesses of the FMSi samples in the intact (0-35% strain) and debonded (100-135% strain) strain regimes.

elongated needle-like formation, as seen in the microscope images in Fig. 1. If the strained composite is held in the strained state and cooled, the deformed FM particles will solidify in place and resist the recovery strain of the matrix upon release from the fixture. This ability to "stretch and hold" a new configuration is referred to as "shape memory" behavior.

We characterized the effect of pre-strain angle (0°, 45°, 90°) and amount of pre-strain (25% and 50%) on the pull-to-failure behavior of FMSi. A pre-strain angle of 0° corresponded to the FM "needles" being aligned with the direction of tension; 90° corresponded to the FM "needles" being perpendicular to the direction of tension. To create samples for these tests, first, films of FMSi were cast. Fabric strips were adhered to the ends, leaving a loop through which rods were threaded. The films were heated in boiling water, stretched to the appropriate amount of strain using the

rods, and held in place using a fixture. After cooling under strain on the fixture to create the elongated FM "needles", rectangular coupons were cut from the film at the appropriate angles and fabric reinforcements were adhered to the ends of each coupon. Five specimens of each treatment were mounted in the materials testing system and pulled to failure at 200% strain/min.

The stress-strain curves from these tests are plotted in Fig. 3A. The no pre-strain samples from Fig. 2 are plotted here as well for comparison. It is apparent that the angle of pre-strain had a significant impact on the initial stiffness of the composite, with the 0° samples being much stiffer than all others, followed by the 45° samples, and then by the 90° samples (Fig. 3B). Interestingly, the 45° samples and the un-pre-strained samples had similar stiffnesses in both the intact and debonded states. All samples appeared to commence their debonded behavior at approximately 70% strain. Notably, the debonding event occurred at approximately the same amount of strain irrespective of the amount or angle of pre-strain, suggesting that this debonding is determined by the matrix-Field's metal interaction, rather than the particulate shape. Following debonding of the matrix from the Field's metal particles, which resulted in a reduction in stiffness by approximately 15x, the differences in stiffness across samples were smaller. Additionally, in the 0° case, an increased amount of pre-strain corresponded to an increase in stiffness, presumably because more of the Field's metal was aligned with the direction of applied strain.

The stiffness values shown in Fig. 3B show that the anisotropic stiffness of FMSi film can be controlled by heating and stretching the film. In the most extreme case shown here (0°-90°, 50% strain), the stiffness difference between the two orthogonal directions was 2.15x. Higher amounts of pre-strain should yield even more skewed differences in stiffness between the axial and transverse directions of applied strain.

D. Shape memory

The shape memory performance of a material can be further characterized by a variety of measures that gauge the effectiveness of the shape change. Noting that some of these values will tend to degrade over time, we repeated these measurements over the course of several days to determine the longevity of the FMSi shape memory effect. The following data was collected from several sheets of FMSi which were heated in boiling water and axially stretched to 100% strain, then cooled in place on a fixture as in the previous section. Before removal from the fixture, several coupons of material 140mm in length and 5mm wide were cut from these sheets and used as the specimens in the tests below.

The primary measure of a shape memory is known as Shape Fixity, which indicates the extent to which the temporary shape is retained. Shape fixity is quantified by the ratio $R_f = \varepsilon/\varepsilon_{load} \cdot 100\%$, for the current strain ε, and the applied strain ε_{load}. Upon being cut out from the fixture, the material specimens experienced some amount of immediate strain relaxation to a length of approximately 120mm,

A

(graph) Shape Fixity (%) vs Days

.... Logarithmic Fit

B

(graph) Shape Recovery (%) vs Days

C

(graph) Recovery stress @100°C (kPa) vs Days
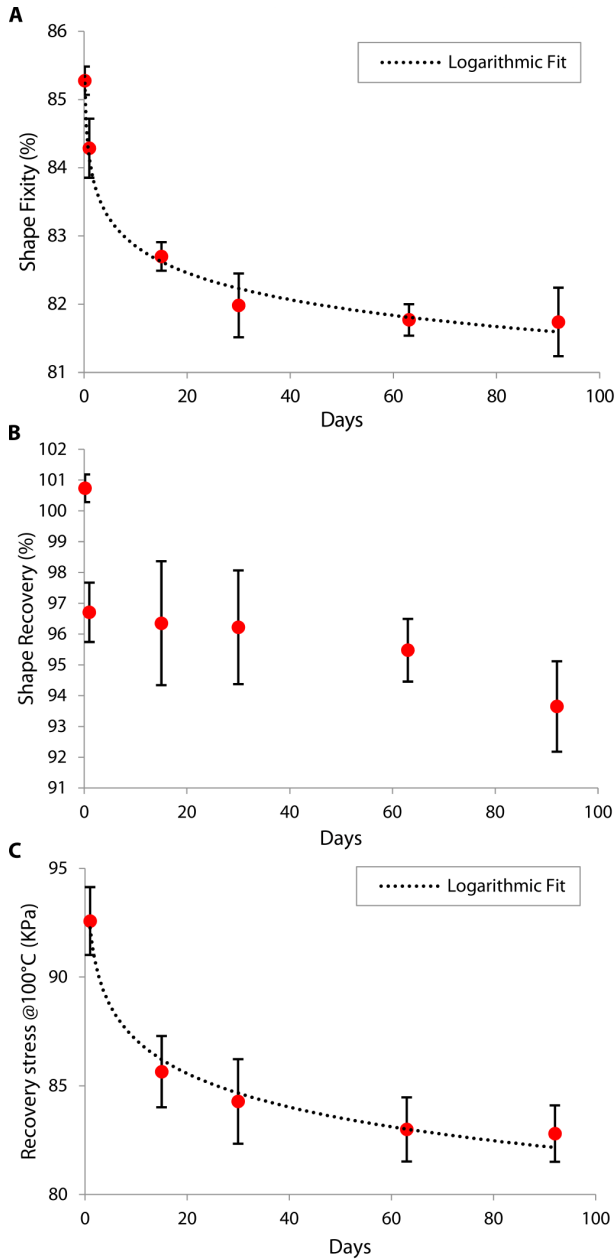
.... Logarithmic Fit

Fig. 4. Shape memory behavior of FMSi and the change over time. Specimens were heated, stretched to 100% strain, cooled in place, and then set aside for the indicated number of days. Error bars show one standard deviation. (A) Shape fixity behavior. 100% shape fixity indicates a specimen remained at its programmed strain without any relaxation. (B) Shape recovery behavior. 100% shape recovery indicates a specimen fully relaxed into its initial unstrained length after heating. (C) Recovery stress of FMSi specimens when heated to 100°C in an isostrain clamp.

resulting in a nominal shape fixity of $R_f = 85.27\%$. We hypothesize that this immediate strain relaxation arises from contraction of silicone. Over time, the material did continue to experience a small additional amount of shape loss in a roughly logarithmic manner, which eventually plateaued to approximately $R_f = 81.98\%$ after about 30 days (Fig. 4A).

Shape Recovery is a measure of how fully the material returns to its original shape after holding the temporary shape for some time. Shape Recovery is defined by the ratio $R_r = \varepsilon_{load} - \varepsilon_{recovered} \cdot 100\%$ where $\varepsilon_{recovered}$ is the remaining strain in the specimen after the recovery transition has occurred. Given the initial nominal strain of 100% and coupon length of 140mm, we calculate that the recovered specimen length should be approximately 70mm. After holding the strained shape for approximately 15 minutes, some samples were heated and allowed to relax freely toward their initial shape. In this case, specimens were measured to have recovered 100.7% of their strain, meaning specimens measured slightly shorter than expected (average length of 69.49mm). Again, the longer the wait time before triggering shape recovery, the less complete that recovery became (Fig. 4B). After about 30 days, this recovery loss accelerates to some degree, possibly indicating permanent creep of the silicone polymer.

A third, interesting feature of shape memory is that of the Recovery Stress, which is a measure of the force with which a material is able to recover its shape. Recovery stress can be measured by holding a specimen in an isostrain fixture and measuring the strain recovery forces as the material is made to transition. This test was performed in a dynamic mechanical analyzer (DMA 850, TA Instruments) in a film tension clamp. Specimens were clamped in the fixture with a torque of 1in-lbs, and heated from 25°C to 55°C at a rate of 5°C/min, at 3°C/min between 55°C and 65°C, and again at 5°C/min to a maximum temperature of 100°C. The resulting blocked forces, after normalization by specimen cross-section into recovery stresses, also appear to follow a logarithmic trend, plateauing after the 30 day mark (Fig. 4C).

III. APPLICATIONS

We demonstrated the shape memory behavior of FMSi material in several applications. All applications have associated video clips (single Supplemental Video file).

A. Variable impedance control of linkage

Noting the change in elastic modulus that can be achieved both by temperature change and by material prestrain, we demonstrate the use of a bar of FMSi as a variable rate spring. The spring is attached to the arm of a pinned linkage, thereby creating a joint with variable impedance which could be used to constrain its motion or manipulate its dynamic response in response to changing loads. We demonstrate three unique cases: an extension spring, a contracting stored-energy actuator, and a combination of the two.

First, the spring is sized to a nominal length of $L_0 = 60$mm. When attached to the linkage, the weight of the arm will stretch the spring to a length of ≈65mm, causing it to hang horizontally and the spring to be oriented at a 45° angle. A 50g weight is loaded onto the arm, causing a small deflection as the spring extends further. The spring is then heated, which allows the arm to drop significantly further under the load. Allowing the spring to cool in this position locks in a new spring constant that will deflect to the same position when loaded with the same weight (Fig. 5A).

Second, the spring is reheated and stretched to $L_0 = 120$mm, a strain of 100%, and cooled in place. After
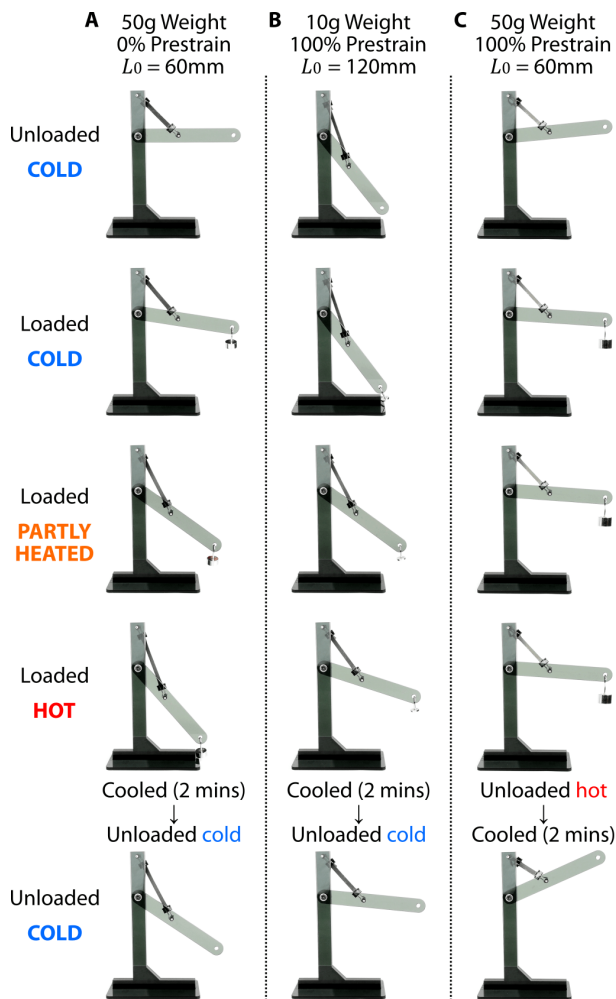
Fig. 5. FMSi used as a variable-impedance spring on a linkage joint. L_0 is the nominal spring length before attachment to the linkage. (A) Acting as an extension spring, the FMSi will change stiffness when heated. Under a 50g load, the linkage will deflect to different points depending on the state of the FMSi. (B) Acting as a contracting actuator, the prestrained FMSi is able to lift a 10g load when heated and allowed to relax toward its unstrained shape. (C) The prestrained FMSi is shortened, allowing it to function as a stiffer extension spring under a 50g load. However, when heated and unloaded, the FMSi will relax and actuate.

attaching to the linkage, a 10g weight is loaded onto the arm, causing a small deflection. The spring is then heated, but rather than deflect further, the FMSi acts as a contracting spring and is able to lift the weight. When cooled in this position, the spring contracts further after removal of the weight (Fig. 5B).

Third, the spring is again reheated and stretched to a strain of 100% and cooled in place. The clips holding the spring are adjusted such that the spring is once again the original length ($L_0 = 60$mm). When attached to the linkage, the higher spring rate caused by the prestrain prevents the arm from hanging horizontally under its own weight. A 50g weight is loaded onto the arm, causing a small deflection as the spring extends. When heated, the spring experiences negligible deflection, as it is already highly strained. Removing the load causes the beam to lift as the spring contracts (Fig. 5C).
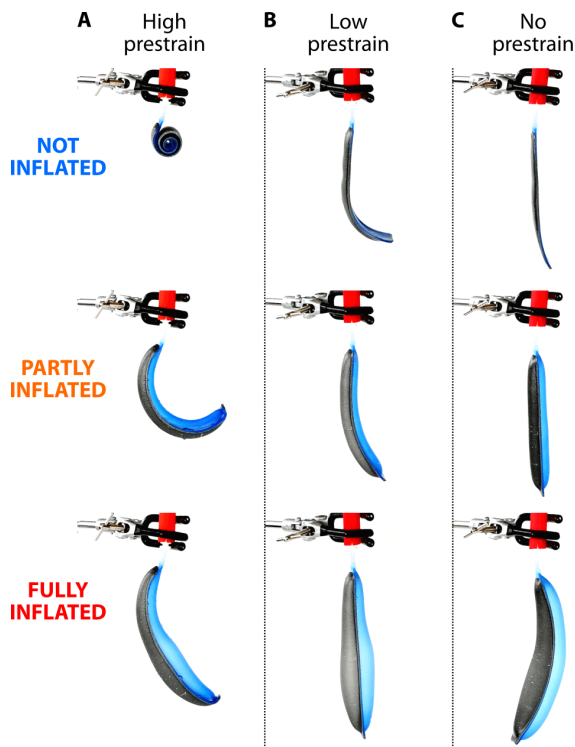

Fig. 6. The inflation trajectory of a bladder with opposing FMSi and neat silicone faces can be controlled by varying the prestrain in the FMSi face. The inflation pressure is 10kPa in all cases. (A) When the FMSi face holds a high prestrain, the strain mismatch causes the bladder to curl. Inflation favors curvature toward the neat silicone layer. (B) A lower prestrain in the FMSi allows the bladder to inflate to a straight shape where the stress is even between the two faces. (C) Zero prestrain in the FMSi causes the bladder to inflate with curvature toward the FMSi face, as it acts as a strain-limiting layer.

B. Soft body trajectory control

FMSi's ability to memorize a strained position can also be used to for soft body trajectory control. Inspired by published works which utilize strain-limiting lamina to direct motion [33], we use an inflatable bladder formed from a sheet of neat Dragonskin 10 silicone and a sheet of FMSi.

In the first case, we heat the FMSi face and apply a large ($\approx 100\%$) strain to the bladder which is then cooled in place. Upon release, the strain mismatch between the two faces causes the bladder to curl up into a tight roll. When inflated, the bladder unrolls and achieves a curved shape, bending toward the neat silicone face (Fig. 6A).

If the bladder is reheated while remaining inflated, the FMSi will relax further until the stress between the two faces is equal, and the bladder will straighten. When the FMSi is cooled at this strain, the bladder can be deflated and reinflated to the same straightened position (Fig. 6B).

When the bladder is deflated and reheated a final time, the FMSi will fully relax, and both faces will be unstrained. When cooled again, the FMSi will act as a strain limiting layer due to its higher stiffness compared to neat silicone. Inflating will now cause the bladder to curve in the opposite direction, toward the FMSi face (Fig. 6C).
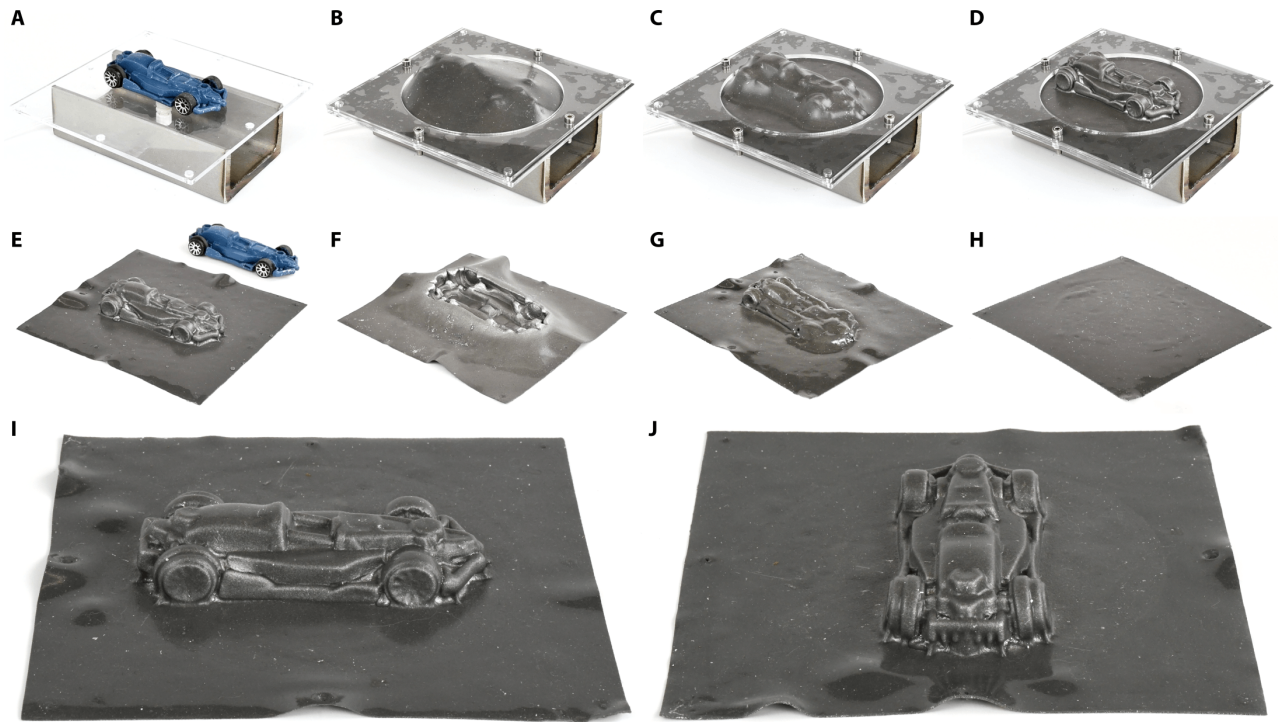
Fig. 7. Detailed topography recording via vacuum forming around a 3D object. (A) The chosen 3D object is placed on the vacuum forming platform. (B) A film of FMSi is secured over the object with a frame bolted into the platform. (C) After heating the film, a vacuum is applied. (D) The film forms tightly about the object, and is allowed to cool in place, memorizing the new shape. (E) The film and object are removed from the platform. The FMSi film retains its shape without requiring any support from the object. (F) Details on the inner surface of the film can be examined. (G) As heat is once again applied, the Field's metal in the film melts. (H) The film returns to its original fully flat shape, read to be reused on a new object. (I-J) The FMSi film is able to record highly detailed features. The square film has an edge length of 6in (15.24cm).

C. Topography recording

Beyond memorizing simple unidirectional strains, FMSi is capable of recording the topography of highly detailed shapes with precise, localized strains distributed throughout the material. This can be clearly demonstrated by using FMSi to assume a complex 3D shape by vacuum forming it around a chosen object.

First the 3D object to be recorded (in this case, a toy car) is placed on a vacuum forming platform, where a film of FMSi is then stretched over and secured in place using an acrylic frame (Fig. 7A-B). The film is then heated thoroughly. With the Field's metal fully melted, a vacuum is pulled to conform the FMSi film to the surface of the object (Fig. 7C-D). With the vacuum pressure maintained, the FMSi is then allowed to cool thereby "memorizing" the surface contours. Once cooled, the frame can be separated and the 3D object is removed from the FMSi. The FMSi film remains highly flexible and stretchable, but the dense structural detail of the memorized FMSi shape allows it to stand under its own weight (Fig. 7E-F). The film can then be heated again to reset it to a flat configuration (Fig. 7G-H), where it can be reused again. The fine features of the toy car were recorded at a high fidelity, with intricate details on the order of 0.5-1mm able to be captured by the FMSi film (Fig. 7I-J).

The particular application of reusable, stretchable, flexible vacuum forming sheets allows for extremely fast creation of molds of objects without expending large volumes of material which must then be cured. However, the general principle of localized strain memorization opens up possible uses in highly specialized trajectory control, complex on-demand spring design, or multi-directional stored-energy actuation in a single material sheet.

IV. CONCLUSIONS

Field's metal particles embedded in silicone yield a stretchable composite with shape memory capabilities. The relatively low-temperature solid-liquid melting transition of the Field's metal is used to reversibly record high-strain deformations. Straining the material to varying levels or in different orientations results in the creation of anisotropic mechanical properties which can then be locked in. The composite is able to retain a memorized shape and recover its initial shape with little change in performance even after months. By varying the order of heating, applying loads, and cooling, a single specimen can leverage its shape memory capability to serve a variety of functions. We show applications where the specimen can act in separate instances as an extension or a compression spring, and dictate the trajectory of an inflated soft body. Additionally, the material can be used to capture topographies, a form of on-demand shape reconfiguration.

We suspect that the on-demand switching of material behavior has applications in other areas as well, from adjustable

damping buffers, to programmable inflatable patterns for pneumatic actuation. This material may even be applicable to wearables and rehabilitative equipment, where stretch and flexibility is paramount, but localized regions of high stiffness can provide needed joint support.

To maximize impact and utility, future work aims to integrate FMSi with similarly stretchable, onboard heating elements. Conductive composites using graphite [8] or liquid metal [10], [34] are candidate materials that could work as addressable heaters to locally melt Field's metal particles, and may even make use of the natural conductivity of FM to Joule heat FMSi directly. Future work should also address the cyclability of the material, in terms of strain cycles in an isothermal state, and in terms of shape memory cyclability.

REFERENCES

[1] J. Mohd Jani, M. Leary, A. Subic, and M. A. Gibson, "A review of shape memory alloy research, applications and opportunities," *Materials & Design*, vol. 56, pp. 1078–1113, Apr. 2014.

[2] L. Hines, K. Petersen, G. Z. Lum, and M. Sitti, "Soft Actuators for Small-Scale Robotics," *Advanced Materials*, vol. 29, no. 13, p. 1603483, 2017.

[3] M. Amjadi, K.-U. Kyung, I. Park, and M. Sitti, "Stretchable, Skin-Mountable, and Wearable Strain Sensors and Their Potential Applications: A Review," *Advanced Functional Materials*, vol. 26, no. 11, pp. 1678–1698, 2016.

[4] D. Buenger, F. Topuz, and J. Groll, "Hydrogels in sensing applications," *Progress in Polymer Science*, vol. 37, pp. 1678–1719, Dec. 2012.

[5] T. Chenal, J. Case, J. Paik, and R. Kramer, "Variable stiffness fabrics with embedded shape memory materials for wearable applications," in *2014 IEEE/RSJ International Conference on Intelligent Robots and Systems (IROS 2014)*, pp. 2827–2831, Sept. 2014.

[6] L. Wang, Y. Yang, Y. Chen, C. Majidi, F. Iida, E. Askounis, and Q. Pei, "Controllable and reversible tuning of material rigidity for robot applications," *Materials Today*, vol. 21, pp. 563–576, June 2018.

[7] S. Araby, Q. Meng, L. Zhang, I. Zaman, P. Majewski, and J. Ma, "Elastomeric composites based on carbon nanomaterials," *Nanotechnology*, vol. 26, no. 11, p. 112001, 2015.

[8] R. A. Bilodeau, M. C. Yuen, and R. Kramer-Bottiglio, "Addressable, Stretchable Heating Silicone Sheets," *Advanced Materials Technologies*, vol. 4, p. 1900276, Sept. 2019.

[9] M. Park, J. Park, and U. Jeong, "Design of conductive composite elastomers for stretchable electronics," *Nano Today*, vol. 9, pp. 244–260, Apr. 2014.

[10] A. Fassler and C. Majidi, "Liquid-Phase Metal Inclusions for a Conductive Polymer Composite," *Advanced Materials*, vol. 27, no. 11, pp. 1928–1932, 2015.

[11] M. D. Bartlett, N. Kazem, M. J. Powell-Palm, X. Huang, W. Sun, J. A. Malen, and C. Majidi, "High thermal conductivity in soft elastomers with elongated liquid metal inclusions," *Proceedings of the National Academy of Sciences*, p. 201616377, Feb. 2017.

[12] S. Yim and M. Sitti, "Design and Rolling Locomotion of a Magnetically Actuated Soft Capsule Endoscope," *IEEE Transactions on Robotics*, vol. 28, pp. 183–194, Feb. 2012.

[13] G. Z. Lum, Z. Ye, X. Dong, H. Marvi, O. Erin, W. Hu, and M. Sitti, "Shape-programmable magnetic soft matter," *Proceedings of the National Academy of Sciences*, vol. 113, pp. E6007–E6015, Oct. 2016.

[14] A. Miriyev, K. Stack, and H. Lipson, "Soft material for soft actuators," *Nature Communications*, vol. 8, pp. 1–8, Sept. 2017.

[15] M. Farshad and A. Benine, "Magnetoactive elastomer composites," *Polymer Testing*, vol. 23, pp. 347–353, May 2004.

[16] P. Testa, R. W. Style, J. Cui, C. Donnelly, E. Borisova, P. M. Derlet, E. R. Dufresne, and L. J. Heyderman, "Magnetically Addressable Shape-Memory and Stiffening in a Composite Elastomer," *Advanced Materials*, vol. 31, p. 1900561, July 2019.

[17] X. Luo and P. T. Mather, "Preparation and Characterization of Shape Memory Elastomeric Composites," *Macromolecules*, vol. 42, pp. 7251–7253, Oct. 2009.

[18] W. Shan, S. Diller, A. Tutcuoglu, and C. Majidi, "Rigidity-tuning conductive elastomer," *Smart Materials and Structures*, vol. 24, no. 6, p. 065001, 2015.

[19] I. M. V. Meerbeek, B. C. M. Murray, J. W. Kim, S. S. Robinson, P. X. Zou, M. N. Silberstein, and R. F. Shepherd, "Morphing Metal and Elastomer Bicontinuous Foams for Reversible Stiffness, Shape Memory, and Self-Healing Soft Machines," *Advanced Materials*, vol. 28, pp. 2801–2806, Apr. 2016.

[20] B. S. Chang, R. Tutika, J. Cutinho, S. Oyola-Reynoso, J. Chen, M. D. Bartlett, and M. M. Thuo, "Mechanically triggered composite stiffness tuning through thermodynamic relaxation (ST3r)," *Materials Horizons*, Jan. 2018.

[21] S.-H. Byun, J. Y. Sim, Z. Zhou, J. Lee, R. Qazi, M. C. Walicki, K. E. Parker, M. P. Haney, S. H. Choi, A. Shon, G. B. Gereau, J. Bilbily, S. Li, Y. Liu, W.-H. Yeo, J. G. McCall, J. Xiao, and J.-W. Jeong, "Mechanically transformative electronics, sensors, and implantable devices," *Science Advances*, vol. 5, p. eaay0418, Nov. 2019.

[22] A. Lendlein and S. Kelch, "Shape-Memory Polymers," *Angewandte Chemie International Edition*, vol. 41, no. 12, pp. 2034–2057, 2002.

[23] I. A. Rousseau and P. T. Mather, "Shape Memory Effect Exhibited by Smectic-C Liquid Crystalline Elastomers," *Journal of the American Chemical Society*, vol. 125, pp. 15300–15301, Dec. 2003.

[24] J. Zhou, S. A. Turner, S. M. Brosnan, Q. Li, J.-M. Y. Carrillo, D. Nykypanchuk, O. Gang, V. S. Ashby, A. V. Dobrynin, and S. S. Sheiko, "Shapeshifting: Reversible Shape Memory in Semicrystalline Elastomers," *Macromolecules*, vol. 47, pp. 1768–1776, Mar. 2014.

[25] J. Li, W. R. Rodgers, and T. Xie, "Semi-crystalline two-way shape memory elastomer," *Polymer*, vol. 52, pp. 5320–5325, Oct. 2011.

[26] Y. Zhu, J. Hu, H. Luo, R. J. Young, L. Deng, S. Zhang, Y. Fan, and G. Ye, "Rapidly switchable water-sensitive shape-memory cellulose/elastomer nano-composites," *Soft Matter*, vol. 8, no. 8, pp. 2509–2517, 2012.

[27] F. Yang, A. Cholewinski, L. Yu, G. Rivers, and B. Zhao, "A hybrid material that reversibly switches between two stable solid states," *Nature Materials*, vol. 18, pp. 874–882, Aug. 2019.

[28] Y. Liu, J. Genzer, and M. D. Dickey, ""2d or not 2d": Shape-programming polymer sheets," *Progress in Polymer Science*, vol. 52, pp. 79–106, Jan. 2016.

[29] J. W. Boley, W. M. van Rees, C. Lissandrello, M. N. Horenstein, R. L. Truby, A. Kotikian, J. A. Lewis, and L. Mahadevan, "Shape-shifting structured lattices via multimaterial 4d printing," *Proceedings of the National Academy of Sciences*, p. 201908806, Oct. 2019.

[30] A. Sydney Gladman, E. A. Matsumoto, R. G. Nuzzo, L. Mahadevan, and J. A. Lewis, "Biomimetic 4d printing," *Nature Materials*, vol. advance online publication, Jan. 2016.

[31] C. Zhang, J.-W. Su, H. Deng, Y. Xie, Z. Yan, and J. Lin, "Reversible Self-Assembly of 3d Architectures Actuated by Responsive Polymers," *ACS Applied Materials & Interfaces*, vol. 9, pp. 41505–41511, Nov. 2017.

[32] T. L. Buckner, M. C. Yuen, S. Y. Kim, and R. Kramer-Bottiglio, "Enhanced Variable Stiffness and Variable Stretchability Enabled by Phase-Changing Particulate Additives," *Advanced Functional Materials*, vol. 0, p. 1903368, Nov. 2019.

[33] S. Y. Kim, R. Baines, J. Booth, N. Vasios, K. Bertoldi, and R. Kramer-Bottiglio, "Reconfigurable soft body trajectories using unidirectionally stretchable composite laminae," *Nature Communications*, vol. 10, pp. 1–8, Aug. 2019.

[34] C. J. Thrasher, Z. J. Farrell, N. J. Morris, C. L. Willey, and C. E. Tabor, "Mechanoresponsive Polymerized Liquid Metal Networks," *Advanced Materials*, vol. 31, no. 40, p. 1903864, 2019.